JMEPEG (2022) 31:3382–3391
https://doi.org/10.1007/s11665-021-06456-y

1059-9495/$19.00

TECHNICAL ARTICLE

Effect of Warm Compaction and Lubricant on Microstructure and Properties of Iron-Based Alloy

Xiaobin Hu, Zili Liu, Xiqin Liu, Huanjian Xie, Cheng Zhang, and Yuwen Zou

Submitted: 27 April 2021 / Revised: 23 October 2021 / Accepted: 5 November 2021 / Published online: 1 December 2021

Lubricant plays an important role in warm compaction technology. This paper investigates the effects of the warm compaction parameters and the lubrication properties of a compound lubricant (polyoxyethylene/bispolyether amide/polyamide) on the microstructure and properties of iron-based powder metallurgy materials. The results showed that the density of the sample containing the compound lubricant was higher than that of the sample containing zinc stearate by 0.1 g/cm^3. With the increase in compaction temperature, the density, bending strength, and dimensional deformation increased and then decreased. The effect of additive amount on performance showed a similar trend. The increase of polyoxyethylene content in the compound lubricant was beneficial to reduce the optimum temperature, but excess polyoxyethylene had an adverse effect on lubrication performance due to fewer functional groups. The optimal parameters of the compound lubricant were a doping ratio of 1:2:2 (polyoxyethylene/dioleic acid amide/polyamide), a lubricant concentration of 0.5%, and a compaction temperature of 140 °C. Under the optimized process parameters, the viscous lubricant could be uniformly distributed in the mixing fraction, and the friction force was reduced to the greatest extent.

Keywords compound lubricant, performance, powder metallurgy, warm compaction

1. Introduction

Powder metallurgy (PM) is a near-net-shape technology for effectively manufacturing parts at lower costs. In recent years, PM has been widely used in automotive, aerospace, biomedical, and other fields (Ref 1-3). The extensive application of PM is mainly attributed to the advancement of new processes, such as warm compaction (Ref 4), hot isostatic pressure (Ref 2), and high velocity compaction (Ref 5). Among them, warm compaction can be combined with die wall lubrication compaction, high velocity compaction, and other techniques to obtain better performance.

Warm compaction requires heating the powder and die assembly above room temperature (Ref 6). The densification mechanism of warm compaction is identical to cold compaction in essence, both of which depend on the rearrangement and plastic deformation of powder particles (Ref 7, 8). During the initial compaction phase, the particle rearrangement effect is dominant due to the large gaps between particles. Subsequently, because of the strong interaction from adjacent particles and the compaction pressure, the particles undergo plastic deformation, which becomes the main driver of densification. However, during the process of particle movement and plastic deformation, friction between particles inevitably exists, which hinders the densification of the parts (Ref 6). Although Rahman (Ref 9) pointed out that the friction coefficient between particles would decrease under compaction temperature, it had no obvious effect on reducing of overall friction. Therefore, adding appropriate lubricant is a necessary condition for high performance.

The addition of lubricant can efficiently decrease friction during the compaction phase, which improves the powder mobility and leads to better compaction density (Ref 10, 11). Compared with cold compaction, the lubricant used in warm compaction is usually a polymer with certain properties, as follows. (1) Relatively low vitrification or melting temperature. Previous studies have found that warm compaction does not significantly improve product performance at temperatures below 100 °C and will enhance the risk of particle oxidation at above 160 °C (Ref 12, 13). Hence, optimal temperature of the lubricant is approximately 100-160 °C, at which temperature the lubricant should be in a viscous state to cover the particle surface. Polystyrene, polyamide, polytetrafluoroethylene, and ethylene bisstearamide are common lubricants in warm compaction (Ref 14-16). (2) Better lubrication performance. Compared with a single lubricant, lubricant mixed with various polymers can achieve better lubrication performance due to complementary advantages. The Hoganas Company developed functional polyolefin lubricants that can be used to manufacture parts with a green density of 7.24 g/cm^3 at a pressure of 700 MPa (Ref 17). Subsequently, a new compound lubricant prepared by a variety of organic compounds was proposed to allow the sintering density of products to reach 7.50 g/cm^3

Xiaobin Hu, Zili Liu, Xiqin Liu, Huanjian Xie, and **Cheng Zhang**, College of Material Science & Technology, Nanjing University of Aeronautics and Astronautics, Nanjing 210016, People's Republic of China; and Jiangsu Automobile Powder Metallurgy Engineering Technology Research Center, Changshu 215534, People's Republic of China; and **Yuwen Zou**, Jiangsu Automobile Powder Metallurgy Engineering Technology Research Center, Changshu 215534, People's Republic of China; and Changshu HuaDe Powder Metallurgy Co, Ltd, Changshu 215534, People's Republic of China. Contact e-mail: liuzili@nuaa.edu.cn.

under the same pressure (Ref 18). The research results by Liu (Ref 19) and Huang (Ref 20) et al. also support this point. (3) Reduce the amount of lubricant to as little as possible. Excessive lubricant is detrimental to its removal at sintering stage, and residual lubricant in the form of gas will increase the porosity. Rahman (Ref 21, 22) and Feng (Ref 16) studied the amount of lubricant and pointed out that the amount of additive of a single lubricant is generally in the range of 0.4∼0.7%. Apart from these characteristics, environmental protection and short burnout cycles are also integrant.

In this paper, a new type of special compound lubricant (polyoxyethylene/bisoleate amide/polyamide) for warm compaction is presented, and its lubrication mechanism is intensely analyzed. In addition, the influences of temperature, additive amount, and other key parameters on performance were studied. Finally, an orthogonal experiment was used to obtain the optimum experimental parameters.

2. Experimental

2.1 Preparation of Mixed Powder

In this experiment, Fe-1.8 Ni-0.5 Mo pre-alloy, 1.5% Cu, 0.5% C, and a self-made compound lubricant consisting of low-density oxidized polyethylene wax (PEOW), ethylene bisoleate amide wax (EBOW), and polyamide wax (PAW) were used as the raw materials. Samples of Fe-based PM materials were prepared by powder mixing, pressing, and sintering. Table 1 shows the composition of the mixed powder. PEOW, EBOW, and PAW were added to the four cans of the mixer in mass ratios of 1:2:2, 2:3:3, and 3:1:1, and then mixed at a speed of 300 rpm for 60 min to produce the compound lubricants A1, A2, and A3, respectively. Then, in a planetary ball mill, Fe-1.8 Ni-0.5 Mo pre-alloy powder, Cu, C, and the self-made composite lubricant were mixed with a ball material ratio of 1:1 and rotated at a speed of 300 rpm for 60 min to obtain the mixed powder. The amount of lubricant added was 0.4, 0.5, 0.6, and 0.7 wt.%. In the present study, zinc stearate (B) was used as a comparison sample.

2.2 Pressing and Sintering

The mold was heated by a temperature-control heating plate. When the temperature of the inner wall of the mold reached the set temperature, as indicated by a TD1100 high-temperature infrared thermometer, the mold was filled with 15.5 g of the mixed powder and kept warm for a period. When the temperature of the mixed powder reached the experimental temperature, a FY-40-II micro tablet press was used to perform unidirectional pressing at a pressure of 600 MPa and held for 60 s to obtain the billet sample (30 × 12 × 6 mm). The pressing temperature range was 25-160 °C.

The billets were placed into the RCWJ-24 sintering furnace under a protective atmosphere (10 vol.% H_2 + 90 vol.% N_2). The whole process includes three stages: pre-sintering, high-temperature sintering, and cooling. First, they were heated to 600 °C at a rate of 20 °C/min and held isothermally for 20 min. Then they were heated to 1200 °C/min at a rate of 20 °C/min and held isothermally for 60 min. Finally, the sintered samples were obtained after being cooled in the furnace.

Table 1 Composition of powder (wt.%)

Ni	Cu	Mo	C	Lubricant	Fe
1.8	1.5	0.5	0.5	0.4-0.7	Balance

2.3 Characterization and Testing

The morphologies of the sintered samples were analyzed using a Hitachi S-4800 scanning electron microscope (SEM) and a BX41M-LED optical microscope (OM). The densities of the sintered specimens were measured by a DH-300 direct reading electrohydrometer according to the Archimedes principle. The bending strength was measured by a three-point bending loading test. The size change percentage (d_{DG}) is defined as $d_{DG} = [(d_G - d_D)/d_D]$ 100%, where d_G and d_D are the sintering size and mold internal size, respectively. Fourier infrared spectrometry was adopted to measure the functional groups of the lubricant.

3. Results and Discussion

3.1 Mixed Powder and Lubricant

Figure 1 shows the density of the metal powder without lubricant at different compaction temperatures (25, 50, 80, 100, 120, 140, and 160 °C). Since high pressure weakens the effect of temperature on performance, an intuitive comparison effect does not appear. Therefore, 500 MPa was adopted for the compaction performance tests. The density trend can be approximately divided into three stages. First, the density did not increase significantly when the temperature was below 50 °C. Then, there was a clear upward trend with the rise of the experimental temperature. Finally, the fluctuation range was small when the temperature was greater than 120 °C. Overall, the results indicated that the best temperature range was 120-160 °C. This was mainly due to the decrease in plastic deformation resistance and densification resistance in the warm compaction process. The lower resistance allowed the plastic deformation process to fully progress, and a higher density was obtained. In addition, excessive temperature increased the risk of oxidation of the metal particles.

Figure 2 shows the results of the differential scanning calorimetry (DSC) tests of (a) PEOW, (b) PAW, (c) EBOW, and

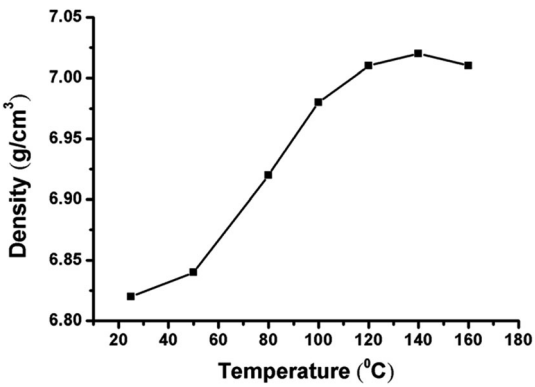

Fig. 1 Variation in density of metal powder without lubricant under different compaction temperatures

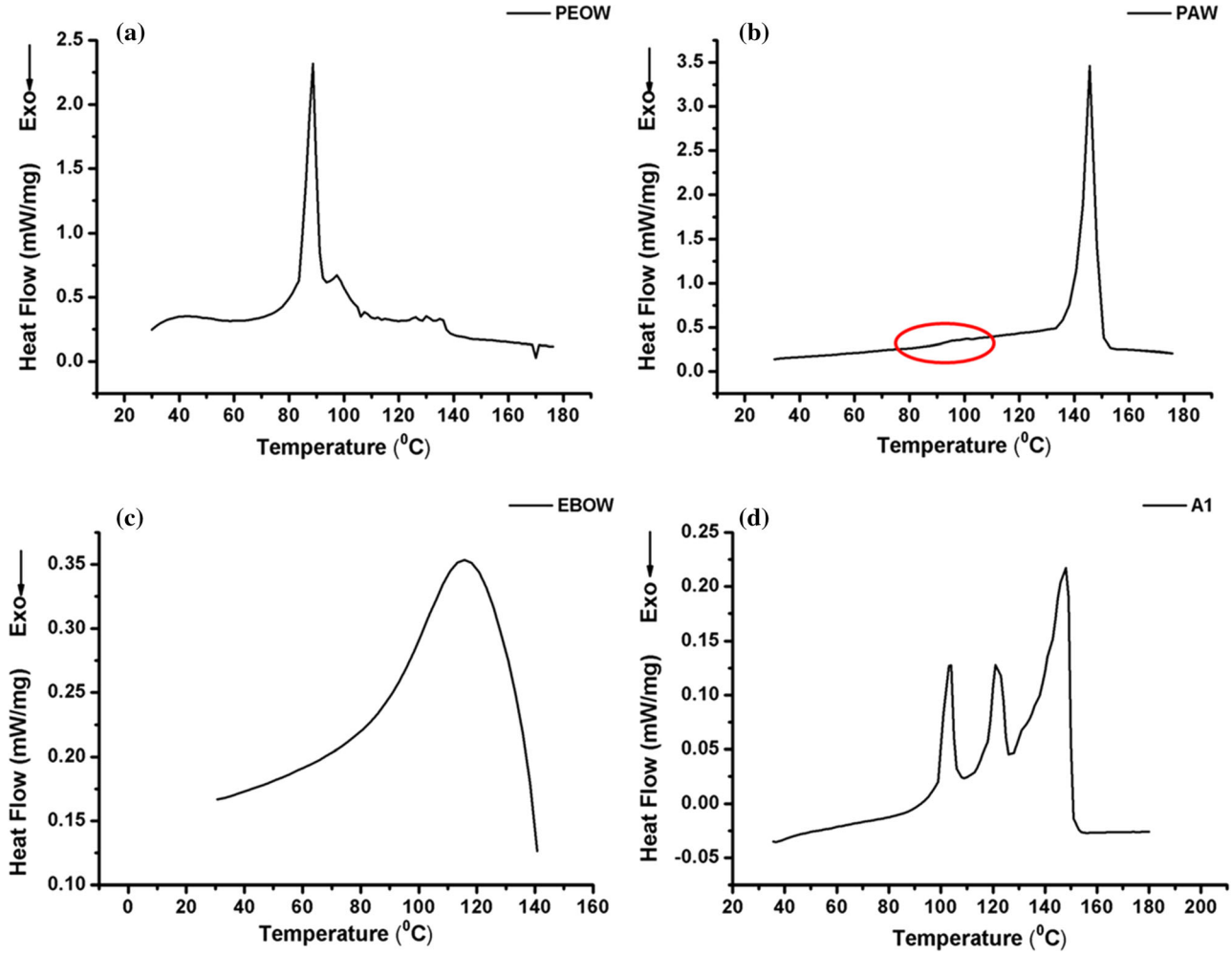

Fig. 2 DSC results: (a) PEOW, (b) PAW, (c) EBOW, and (d) A1

(d) compound lubricant A1. All of the lubricant components and the compound lubricant displayed melting peaks, indicating that part of the lubricant was crystallized. The melting points of PEOW, PAW, and EBOW were approximately 80, 140, and 115 °C, respectively. Only PAW showed an obvious glass transition temperature of approximately 95 °C. Multiple peaks appeared in the test results of compound lubricant A1, which indicates poor compatibility of the three components. An important factor that caused this poor compatibility was the different polarities of the components.

Figure 3 shows the SEM-EDS micrographs of the mixed powder containing compound lubricant A1, from which the size, shape, and distribution of the particles were obtained. The particle size was mainly in the range of 20-75 μm, which indicates that ball milling effectively reduced the particle size of the metal powder. The smaller particle size was effective for dispersion strengthening, which is beneficial for performance improvement. Except for a few nearly spherical particles, most of the mixed powder was irregular, which helps improve the sample density and strength. Because particles are combined by the pressing force during the molding process, irregular particles are more likely to mesh better. Moreover, particles will wedge and hook to each other because of the different concave or convex particle surfaces, which will improve the degree of densification and strength of the samples. Finally, the element analysis of Fig. 3 shows that Ni, Mo, and the lubricant were uniformly distributed in the mixed powder; however, Cu was poorly distributed. Ni and Mo were added in the way of alloying, which contributes to homogenization of the elements. The uneven distribution of Cu occurred mainly because it was added to the mixed powder as pure Cu during ball milling. Moreover, part of large Cu particle increases the likelihood of unevenness. The inhomogeneity may result in the presence of residual austenite at the copper aggregation sites in the sintered samples (Ref 23).

3.2 Effect of Lubricant Type on Sample Properties

Figure 4 and 5 shows the experimental results of the sintering density and bending strength of the samples admixed with different lubricants. The samples containing lubricants A1 and A2 had the highest density at 140 °C. Under the same parameters, the samples with the A3 composite lubricant obtained the highest density at 120 °C, which shows that PEOW was conducive to reducing the compaction temperature of the composite lubricant. Overall, the density of the sample admixed with lubricant A1 was higher than those containing lubricants A2 or A3. The experimental results also showed that the transverse fracture strength was inversely proportional to the ratio of PEOW in the compound lubricant, which indicates that the higher PEOW content in the compound lubricant had

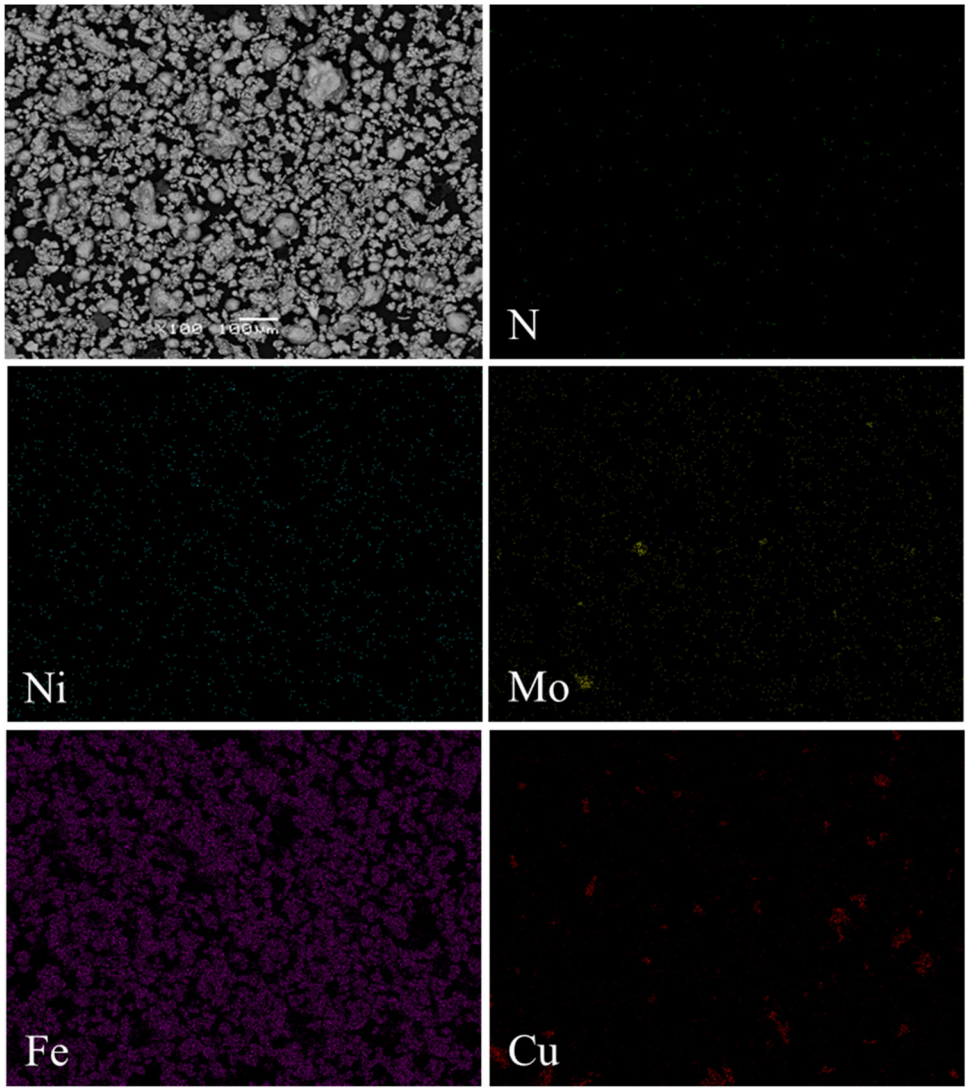

Fig. 3 The SEM-EDS micrographs of the mixed powder containing compound lubricant A1

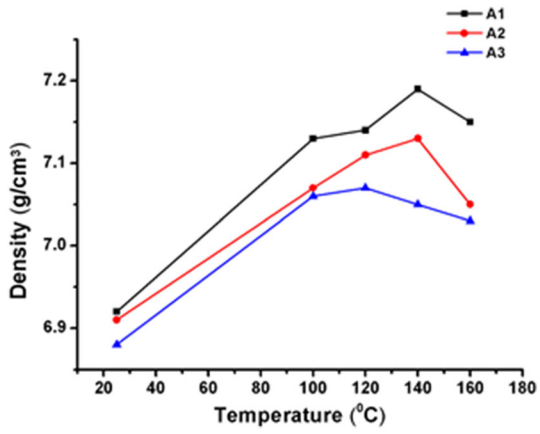

Fig. 4 Variation in density with different lubricants

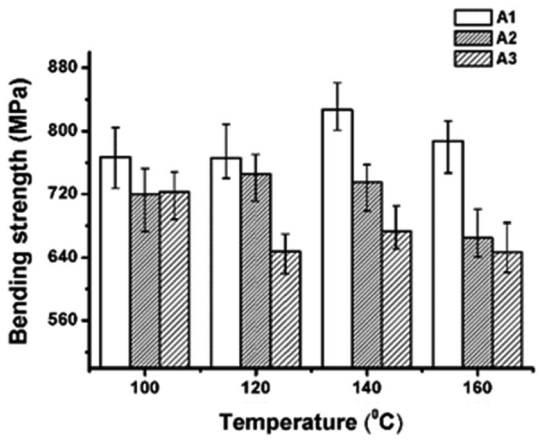

Fig. 5 Variation in bending strength with different lubricants

adverse effects on the sample properties. The properties of the products with different types of lubricants were different at the appropriate compaction temperature and lubricant concentration, which indicates that there are essential differences between the lubricants. These lubricants mainly differ in their molecular chain structure, functional group type, and molecular weight.

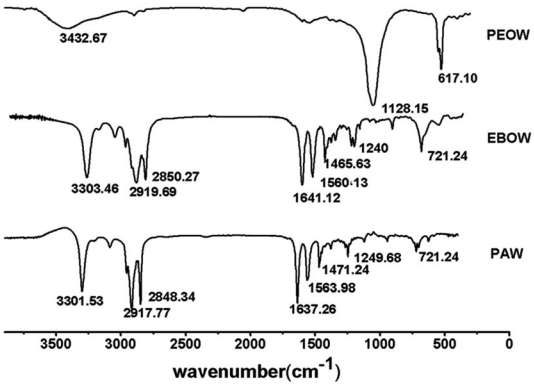

Fig. 6 Infrared spectra of compound lubricant components

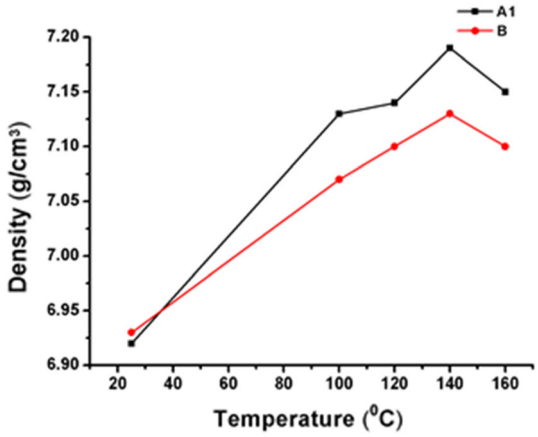

Fig. 7 Variation in density with different compaction temperatures

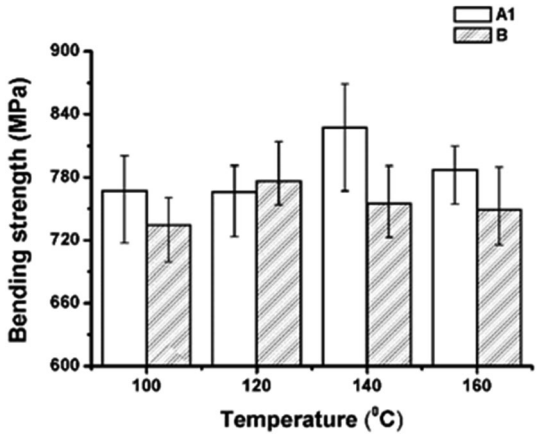

Fig. 8 Variation in bending strength with different compaction temperatures

Figure 6 shows the infrared spectra of the three components of the compound lubricant. PAW and EBOW have similar groups, mainly –NH_2– (3303.53), –CH_2– (2917.77, 2850.27, 721.24), and –CO–NH– (1637.26, 1560.13) (Ref 24, 25). PEOW contains –OH– (3432.67) and –CO– (1128.15) (Ref 26). The adhesion of the lubricant molecules on the metal particle surfaces was mainly based on molecular and chemical bonds.

First, due to the direct contact between the lubricant and metal particle surfaces, there will be intermolecular forces, including hydrogen bond forces and van der Waals forces. Van der Waals forces include electrostatic forces, induction forces, and dispersion forces. Electrostatic force is the force between polar molecules, whereas induction and dispersion forces occur between polar molecules as well as between polar and non-polar molecules. Second, when there are more polar groups in the lubricant, chemical bonds form with the free bonds on the metal surface, thus improving the adhesion ability. Compared with PAW and EBOW, the PEOW used in this experiment contained fewer polar molecules, which would reduce the binding sites between it and the metal particles. When adhesion between the lubricant and the metal particle surfaces is difficult, the lubricant will appear in the gaps between particles during the compaction stage, rather than in contact with the particle. In addition, when the temperature rises during the pressing process, the fluidity of the lubricant is enhanced, and the poor adhesion effect makes the lubricant move to fill some voids. This worsens the lubrication effect, reducing the performance of the sample. In contrast, PAW and EBOW have higher polarity and contain a large number of intermolecular hydrogen bonds, which facilitated adhesion of the lubricant on the metal surface. The better adhesion of the lubricant on the surface of the metal particles facilitated their dispersion to a certain extent, thus improving the lubrication effect.

3.3 Effects of Temperature and Lubricant Concentration on Sample Properties

3.3.1 Temperature. Figure 7 shows the variation in density with different temperatures. Compared with conventional compaction, the warm compaction process can increase the density of the sample by 0.2 g/cm^3. At the same compacting pressure, the density generally increases and then decreases with the increase in temperature (25-160 °C). The samples containing both zinc stearate and the compound lubricant obtained maximum density at approximately 140 °C, but the maximum density of the sample with compound lubricant was nearly 0.1 g/cm^3 higher than that containing zinc stearate. The results of the transverse rupture strength effected by temperature were similar to that of density (Fig. 8).

For the above results, Fig. 9 provides a more detailed explanation. Figure 9 shows a simple diagram of the state of the lubricant during warm compaction. Due to the relatively small size of the lubricant, it sticks to the surface of the metal particles or exists in the particle gaps in the mixed powder at room temperature (Fig. 9(1)). As the temperature rises, the physical state of the lubricant changes significantly (Fig. 9(2)). The spread area of the lubricant on the particle surface increases, which is conducive to reducing the friction among particles. At the same time, the efficiency of the compaction pressure applied to the metal particles is enhanced, which leads to improvement in the degree of densification and mechanical bonding. The properties of the sintered samples also improve. Furthermore, although the die wall lubricated technology was not employed in this experiment, part of the lubricant may be present on the mold wall during pressurization, which would also reduce friction between the particles and the die wall.

Figure 10 illustrates the relationship between the dimensional changes of the sintered samples and the compaction temperature. Figure 10 clearly shows that the dimensional changes of the sample admixed with the compound lubricant

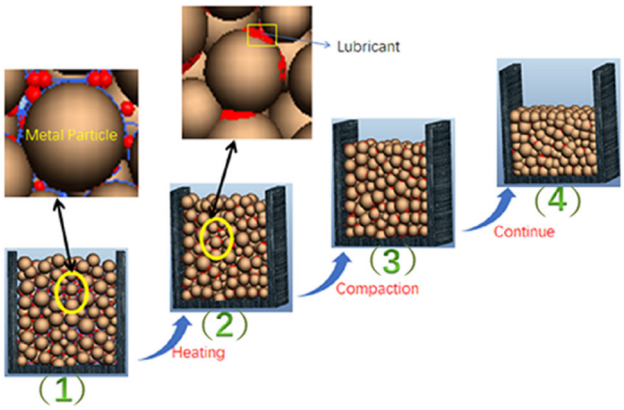

Fig. 9 Variation in lubricants under warm compaction

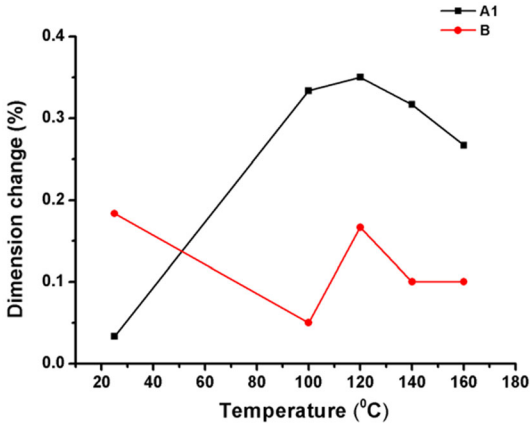

Fig. 10 Variation in dimensional changes with different compaction temperatures

initially increased and then decreased as the temperature rose, whereas the sample containing zinc stearate showed no obvious changes under the same conditions. Therefore, the dimensional stability of the sample with zinc stearate was better than that of the sample containing the compound lubricant. In the current study, the size change mainly occurred because of two processes: the spring back effect after compaction and sintering densification (Ref 27). The spring back effect is the result of spring expansion of the powder particles with plastic deformation when the binding force disappears. The particles are combined by mechanical force, which creates a strong combination between the particles and plays a certain inhibitory effect on the elastic recovery so that the particles cannot expand freely. However, if there is a lubricant between the particles, the bond between the particles is weakened, which will reduce the resistance to elastic aftereffect and eventually increase the deformation rate. Furthermore, the distribution of compound lubricant between metal particles is wider than that of zinc stearate under warm compaction, so elastic aftereffect is more obvious. During the sintering process, lubricant removal and element homogenization diffusion occur, and some pores are filled to make the particles more compact, thus causing dimensional shrinkage. In addition, because of the high densification of the green sample containing compound lubricant, the dimensional shrinkage is smaller under the same sintering conditions.

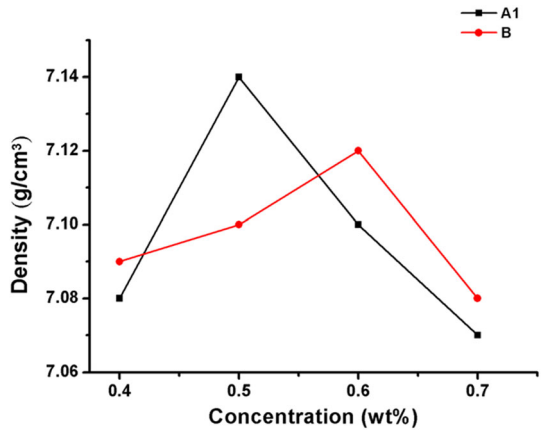

Fig. 11 Variation in density with different concentrations

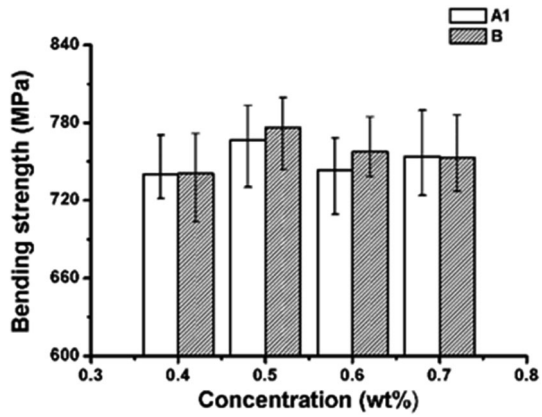

Fig. 12 Variation in bending strength with different concentrations

3.3.2 Concentration. Figure 11 and 12 shows the effect of lubricant concentration on the sintering density and transverse rupture strength, respectively, at 120 °C. The overall trend for the performance of the samples with the two lubricants is the same. In addition, both presented an inverted V-shape, but the amount of lubricant at the vertices does not coincide. The optimal concentration of the compound lubricant (0.5 wt.%) was lower than that of zinc stearate (0.6 wt.%), which is conducive to the removal of lubricant in the sintering stage. In comparison with zinc stearate, the samples containing the compound lubricant exhibited better performance with the addition of less lubricant. In the case of the compound lubricant, when the content is less than 0.5 wt.%, there will be a lack of lubricant at some locations, which may lead to uneven distribution of alloying elements during the pressing process and even make the properties of the sintered samples poor. Compared with the adhesion between metal particles and lubricants, lubricants are more likely to bond to each other. Therefore, when the content is higher than 0.5 wt.%, the metal powder space may be occupied due to the accumulation of lubricant, which leads to the increase in sample pore size and porosity.

Figure 13 shows the pore distribution of the sintered samples with different contents of compound lubricants. It can be seen that the pore shape was irregular (Fig. 13e), which was the result of the slow spheroidization of pores during the sintering process. Due to efficiency and cost considerations, the

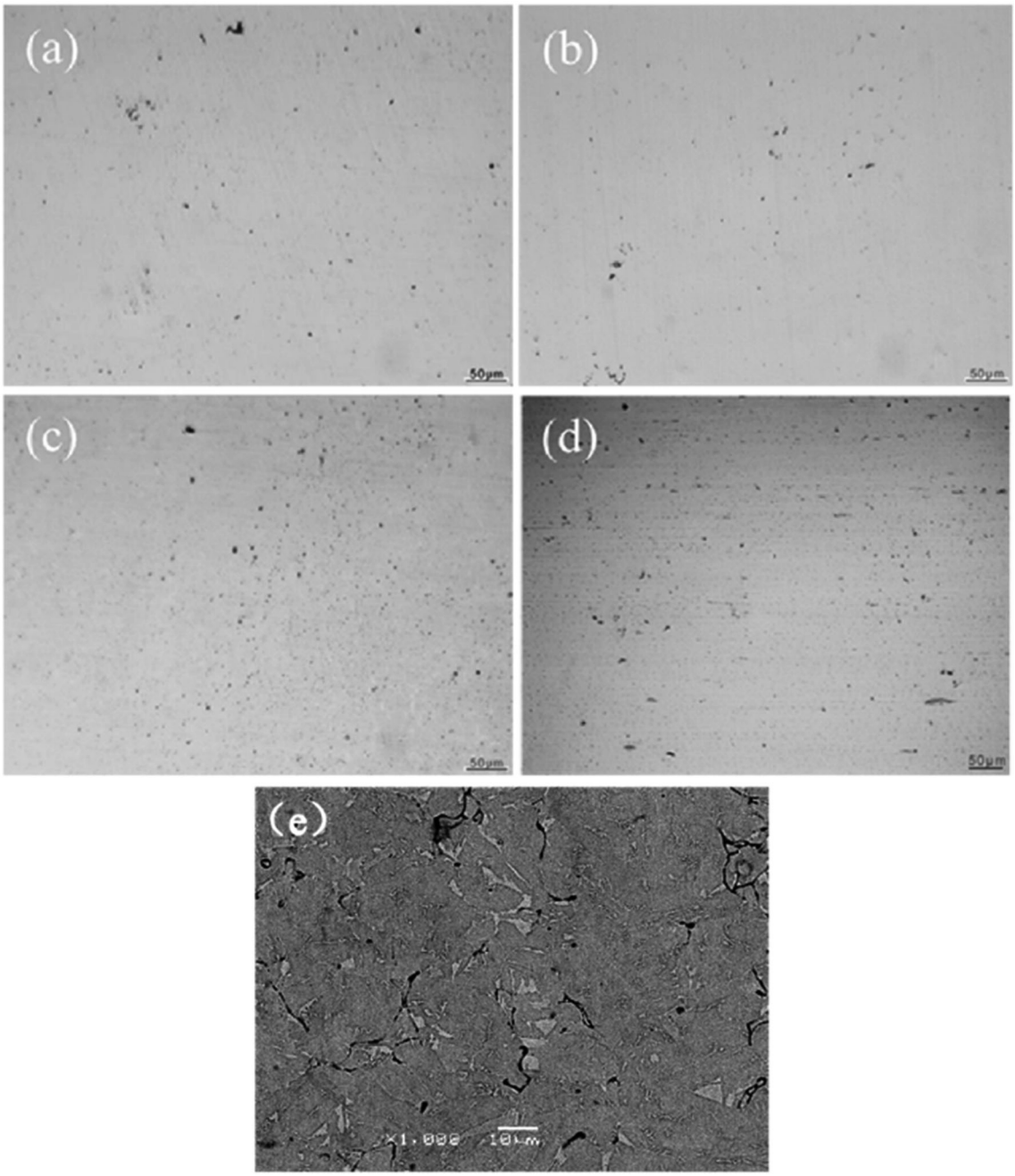

Fig. 13 Pore morphology with different lubricant concentrations: 0.4 wt.%, (b, e) 0.5 wt.%, (c) 0.6 wt.%, and (d) 0.7 wt.%

sintering time could not be extended sufficiently for spheroidization to occur. In addition, transient liquid phase sintering of copper is known to increase the complexity of the pores in the sample (Ref 28). Furthermore, the lubricant content was proportional to the number and size of the pores (Fig. 13a-d). This phenomenon can be viewed from the following perspectives. First, the particles were not completely in contact with each other, increasing the possibility of large pores, especially in the case of improper lubrication. In addition, although removal of the lubricant was performed in the pre-firing stage, residual lubricant may have existed in a gaseous form if the content was too high. Under either of the above conditions, with the continuous increase of sintering temperature, a large number of obturator pores will form and continuously shrink in the subsequent stages. If the pressure of the residual gas in the pores exceeds the surface tension required for pore shrinkage, the shrinkage will cease, and large irregular pores will appear in the sample. In PM parts, the internal pores are the source of crack propagation, and the surface pores reduce adhesion between the coating and matrix (Ref 29).

3.4 Parameter Optimization

Table 2 shows the combination of factor levels of the orthogonal test. Table 3 displays the orthogonal array (L16) of the sample densities obtained at different temperatures, lubricant concentrations, and lubricant types. The range method was used to analyze the orthogonal experimental results. It was

Table 2 Three-factor and four-level orthogonal array

Level	Factors		
	Concentration, wt.%	Temperature, °C	Type
Level one	0.4	100	A1
Level two	0.5	120	A2
Level three	0.6	140	A3
Level four	0.7	160	B

Table 4 EDS analysis of the points in Fig. 14

Point	Ni	Mo	Cu	Fe
A	2.07	1.20	3.62	93.11
B	2.39	1.26	1.88	94.46
C	1.79	0.86	2.73	94.62
D	1.99	1.12	3.06	93.84

Table 3 The orthogonal array L16 (4^3) of sample densities

	Concentration, wt.%	Temperature, °C	Type	Density, g/cm^3
1	0.4	100	A2	7.09
2	0.4	140	A3	7.05
3	0.4	160	A1	7.06
4	0.4	120	B	7.09
5	0.5	100	A3	7.06
6	0.5	140	A1	7.19
7	0.5	160	B	7.1
8	0.5	120	A2	7.11
9	0.6	100	B	7.09
10	0.6	140	A2	7.06
11	0.6	160	A3	7.01
12	0.6	120	A1	7.1
13	0.7	100	A1	7.12
14	0.7	140	B	7.07
15	0.7	160	A2	7.04
16	0.7	120	A3	7.04
k1	7.0725	7.09	7.1175	
k2	7.115	7.085	7.075	
k3	7.065	7.0925	7.04	
k4	7.0675	7.0525	7.0875	
R	0.05	0.04	0.0775	
Optimum parameters	0.5 140 A1			

found that the degree of influence of the experimental parameters on the experimental results ranged from large to small as follows: type of lubricant, amount of additive, and compaction temperature. As observed in Tables 2 and 3, the optimum process parameters were lubricant concentration of 0.5%, compacting temperature of 140 °C, and doping ratio of the PEOW/EBOW/PAW lubricant of 1:2:2 (Table 4).

Figure 14 shows the OM micrographs (a, b) and SEM-EDS micrographs (c, d) of the sintered sample under the optimal parameters. As can be seen from Fig. 14(a), (c), the overall structure of the sample was relatively uniform and was composed of grayish white martensite (M), dark pearlite or bainite (P/B), and bright-white residual austenite (RA). Among them, the martensite content was the largest, which was a result of the faster cooling rate used in the experiment. Usually, the existence of RA is caused by Ni segregation, but according to the test results, there was no obvious uneven distribution of Ni. However, Cu had obvious segregation, which can be reflected in two aspects. First, the Cu distribution in the mixed powder was not uniform (Fig. 3). Second, there was insufficient diffusion in the sintering process. Comparison of the elements at various points in Fig. 14(d) illustrates this idea well. Taking two points (A, B) as an example, the Cu content at point A (3.62 wt.%) was nearly twice that at point B (1.88 wt.%). Therefore, the above results indicate that the existence of RA in this experiment was mainly due to Cu segregation. These results are consistent with the previous expectation that an uneven distribution of Cu in mixed powder might cause consequences.

4. Conclusion

1. The polyoxyethylene content in the compound lubricant was 20%, the optimal operating temperature was 140 °C, and the corresponding density and strength were 7.19 g/cm^3 and 826.9 MPa, respectively. When the content increased to 60%, the corresponding values were 100 °C, 7.06 g/cm^3, and 722.7 MPa, respectively.
2. With the increase in pressing temperature, the sintering density, bending strength, and dimensional deformation of the sample containing the composite lubricant initially increased and then decreased. The effect of additive amount on performance showed the same trend.

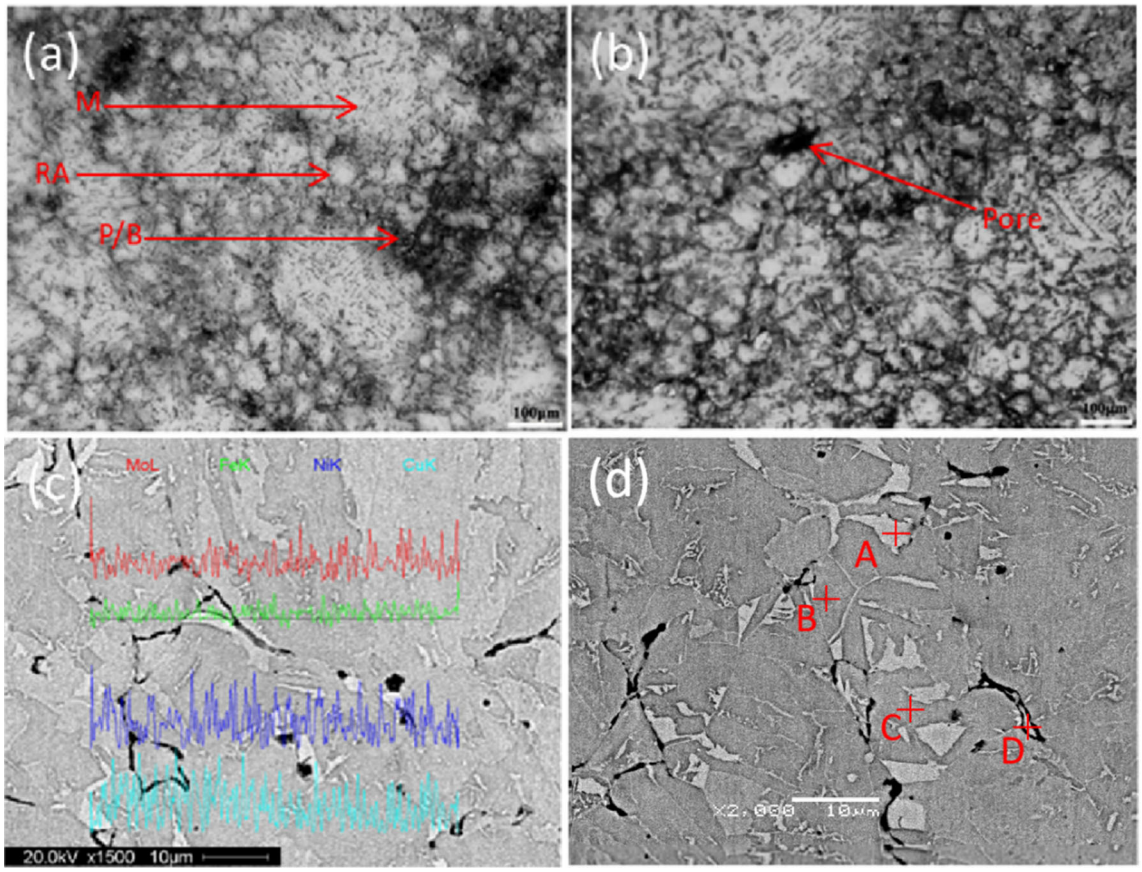

Fig. 14 OM micrographs (a, b) and SEM-EDS micrographs (c, d) of the sample under the optimal parameters

3. At 140 °C, the specimens with 0.5% lubricant A1 (PEOW/EBOW/PAW, 1:2:2) obtained a higher density of 7.19 g/cm^3.

Acknowledgments

This study is financially supported by A Project Funded by the Priority Academic Program Development of Jiangsu Higher Education Institutions.

References

1. J. Capus, Powder Metallurgy, Progress and the Eco-friendly Car, *Metal Powder Rep.*, 2011, **66**(2), p 16–18
2. B. Sreenu, R. Sarkar and S.S. Satheesh Kumar, Microstructure and Mechanical Behaviour of an Advanced Powder Metallurgy Nickel Base Superalloy Processed Through Hot Isostatic Pressing Route for Aerospace Applications, *Mater. Sci. Eng. A*, 2020, **797**, p 140254. https://doi.org/10.1016/j.msea.2020.140254
3. S. Jayasathyakawin, M. Ravichandran and N. Baskar, Magnesium Matrix Composite for Biomedical Applications Through Powder Metallurgy—Review, *Mater. Today. Proceed*, 2020, **27**(2), p 736–741
4. A. Shagil, S. Mohammad, R.M. Mohd and C.S. Manish, Recent Advancements in Powder Metallurgy: A Review, *Mater. Today*, 2018, **5**(9), p 18649–18655
5. C.Y. Tang, Z.Y. Xiao, J. Chen and C.J. Li, Compaction Experiment on the Newly Designed Warm High Velocity Compaction Equipment, *Adv. Mater. R*, 2010, **139**, p 485–488
6. A. Simchi and A.A. Nojoomi, Warm Compaction of Metallic Powders, *Adv. Powder Metall.*, 2013, **5**, p 86–108
7. D.Y. Yoon, S.L.K.Y. Eun and Y.S. Kim, Densification Mechanism of Warm Compaction for Iron-based Powder Materials, *Mater. Sci. Forum*, 2007, p 261-264
8. A. Simchi, Behaviour of Metal Powders During Cold and Warm Compaction, *Powder Metall.*, 2006, **49**(3), p 281–287
9. M.M. Rahman, A.K. Ariffin, S.S.M. Nor and H.Y. Rahman, Powder Material Parameters Establishment Through Warm Forming route, *Mater. Des.*, 2011, **32**(1), p 264–271
10. S.S.M. Nor, M.M. Rahman, F. Tarlochan, B. Shahida and A.K. Ariffin, The Effect of Lubrication in Reducing Net Friction in Warm Powder Compaction Process, *J. Mater. Process. Tech.*, 2007, **207**(1), p 118–124
11. K.E. Ravi, A. Lusin and S. Kumar, Effects of Lubricant on Green Strength, Compressibility and Ejection of Parts in Die Compaction Process, *Powder Technol.*, 2013, **233**(1), p 22–29
12. B. Abolfazl, H. Ali and M. Ghambari, On the Combined Effect of Lubrication and Compaction Temperature on Properties of Iron-Based P/M Parts, *Mater. Sci. Eng. A*, 2006, **437**, p 360–365
13. R. Muresan, Research into the Warm Compaction of Metal Powders, *Mater. Res. Proceed.*, 2018, **8**, p 152–156
14. M.M. Rahman, S.S.M. Nor and H.Y. Rahman, Investigation on the Effect of Lubrication and Forming Parameters to the Green Compact Generated from Iron Powder Through Warm Forming Route, *Mater. Des.*, 2011, **32**, p 447–452
15. Z.Y. Xiao, M.Y. Ke, L. Fang, M. Shao and Y.Y. Li, Die Wall Lubricated Warm Compacting and Sintering Behaviors of Pre-mixed Fe–Ni–Cu–Mo–C Powders, *Mater. Process. Tech.*, 2009, **209**, p 4527–4530
16. S.S. Feng, H.R. Geng and Zh.Q. Guo, Effect of Lubricants on Warm Compaction Process of Cu-Based Composite, *Compos. Part B*, 2012, **43**, p 933–939
17. G. Poszmik. Improved Powder Metallurgy Lubricant Compositions and Methods for Using the Same, US, WO 03/065759A1, 2003
18. G.H. Francis and T. William. Lubricant System for Use in Powder Metallurgy, US, US009533353B2, 2017
19. Z.L Liu, H.H Li and X.Q. Liu, Effect of Warm Compaction Lubricant on the Properties of Fe-Based Powder Metallurgy Materials, *Mater.*

Res. Express, 2019, **6**(04), 046534. https://doi.org/10.1088/2053-1591/aafbfa
20. X. Huang, Z.L. Liu, X.Q. Liu, Z.H. Tang and H.H. Li, Effects of Erucylamide and EBS Composite Lubricant on the Properties of Fe Based Powder and Green Compact, *Mater. Res. Express*, 2017, **4**(10), 116509. https://doi.org/10.1088/2053-1591/aa9323
21. M.M. Rahman and S.S.M. Nor, An Experimental Investigation of Metal Powder Compaction at Elevated Temperature, *Mech. Mater.*, 2008, **41**(5), p 553–560
22. M.M. Rahman, S.S.M. Nor and A.K. Ariffin, Effect of Lubricant Content to the Properties of Fe-Based Components Formed at above Ambient Temperature, *Proced. Eng.*, 2013, **68**, p 425–430
23. S. Wang, Q. Wang and H.L. Wang, Effects of Copper Content on Microstructure and Mechanical Properties of Powder-Forged Rod Fe-C-Cu Alloys Manufactured at Elevated Temperature, *Mater. Sci. Eng. A*, 2019, **743**, p 197–206
24. C.Y. Ji, X.W. Zhang and P.Q. Yu, Using Non-invasive Molecular Spectroscopic Techniques to Detect Unique Aspects of Protein Amide Functional Groups and Chemical Properties of Modeled Forage from Different Sourced-Origins, *Spectrochim. Acta. A*, 2016, **156**, p 151–154
25. B.S. Rao, Synthesis and Characterization of Polyimide-Polyoxyethylene Copolymers Containing Carboxylic Acid Functional Groups, *Eur. Polym. J.*, 1997, **33**(9), p 1529–1536
26. M. Hadri, A. Achahbar, J. Khamkhami, B. Khelif and V. Faivre, Raman Spectroscopy Investigation of Mono- and Diacyl-polyoxyethylene Glycols, *Vib. Spectrosc.*, 2013, **64**, p 78–88
27. A. Vagnon, O. Lame, D. Bouvard, M. Di Michiel, D. Bellet and G. Kapelski, Deformation of Steel Powder Compacts During Sintering: Correlation Between Macroscopic Measurement and In Situ Microtomography Analysis, *Acta Mater.*, 2006, **54**(2), p 513–522
28. J. Kong, C.P. Xu, J.L. Li, W. Chen and H.Y. Hou, Evolution of Fractal Features of Pores in Compacting and Sintering Process, *Adv. Powder Technol.*, 2010, **22**(3), p 39–42
29. M. Etaat, H. Pouraliakbar, G. Khalaj and M. Ghambari, Adhesion Strength Measurement of Nickel Layer on the Iron-Based P/M Parts Influenced by Different Surface Pre-treatment Operations, *Measurement*, 2015, **66**, p 204–211